Yang DW, Shinjiro K, Taikan O, Toshio K, Katumi M. Global potential soil erosion with reference to land use and climate changes…

Article *in* Hydrological Processes · October 2003

DOI: 10.1002/hyp.1441

CITATIONS
194

READS
451

5 authors, including:

Dawen Yang
Tsinghua University
179 PUBLICATIONS **3,134** CITATIONS
SEE PROFILE

Taikan Oki
The University of Tokyo, Meguro-ku, Tokyo, J…
495 PUBLICATIONS **10,756** CITATIONS
SEE PROFILE

HYDROLOGICAL PROCESSES
Hydrol. Process. **17**, 2913–2928 (2003)
Published online in Wiley InterScience (www.interscience.wiley.com). DOI: 10.1002/hyp.1441

Global potential soil erosion with reference to land use and climate changes

Dawen Yang,[1]* Shinjiro Kanae,[2] Taikan Oki,[2] Toshio Koike[1] and Katumi Musiake[2]

[1] *Department of Civil Engineering, University of Tokyo, Tokyo 113-8656, Japan*
[2] *Institute of Industrial Science, University of Tokyo, Tokyo 153-8505, Japan*

Abstract:

A GIS-based RUSLE model is employed to study the global soil erosion potential for viewing the present situation, analysing changes over the past century, and projecting future trends with reference to global changes in land use and climate. Scenarios considered in the study include historical, present and future conditions of cropland and climate. This research gives the first overview of the global situation of soil erosion potential considering the previous century as well as the present and future. Present soil erosion potential is estimated to be about 0·38 mm year^{-1} for the globe, with Southeast Asia found to be the most seriously affected region in the world. It is estimated that nearly 60% of present soil erosions are induced by human activity. With development of cropland in the last century, soil erosion potential is estimated to have increased by about 17%. Global warming might significantly increase the potential for soil erosion, and the regions with the same increasing trend of precipitation and population might face much more serious problems related to soil erosion in the future. Copyright © 2003 John Wiley & Sons, Ltd.

KEY WORDS global change; soil erosion; global warming; land use change; RUSLE

INTRODUCTION

Soil, present in most landscapes of the earth, plays an important role in the natural ecosystem (Singer and Warkentin, 1996), and soil is a major natural life-supporting resource. Soil erosion is a principal degradative process resulting in a decrease in effective root depth, nutrient and water imbalance in the root zone, and reduction in productivity. Soil erosion is a major environmental threat to the sustainability and productive capacity of agriculture. During the last 40 years, nearly one-third of the world's arable land was lost to erosion, with loss continuing at a rate of more than 10 million hectares per year. With the addition of a quarter of a million people each day, the world population's food demand is increasing at a time when per capita food productivity is beginning to decline (Pimentel *et al.*, 1995). Mankind's basic need for food is satisfied through the use of soil, however, soil productivity is being seriously reduced by soil degradation. Among the human-induced causes of soil degradation, erosion by water is the most common type, causing about 55% of total global erosion (Bridges and Oldeman, 1999). Soil erosion has also been recognized to be the major non-point pollution source in many areas, which causes a large amount of damage every year. As an example for the United States, the range of net damage cost of erosion-related pollutants was estimated to be \$3·2–\$13·0 billion in 1980 (Singer and Warkentin, 1996). Soil erosion leads to preferential removal of a soil's organic carbon and clay contents. As much as 20% of carbon transported by eroded sediments may be released into the atmosphere as CO_2 (Lal and Bruce, 1999). Soil erosion is directly related to food productivity reduction and water pollution, and may also reduce the ability of soil to mitigate the greenhouse effect. Soil erosion is a common natural disaster in the world, and local soil erosion processes link with the

* Correspondence to: Dawen Yang, Department of Civil Engineering, University of Tokyo, Tokyo 113-8656, Japan.
E-mail: dyang@hydra.t.u-tokyo.ac.jp

Received 16 May 2002
Accepted 23 February 2003

global biosphere system and global cycles, such as water and substance cycles. For a better understanding of global environmental issues, it is desirable to have a global view of past and present soil erosion, and a projection of future soil erosion. Soil erosion includes mainly water erosion and wind erosion, however only water erosion is simulated and discussed in this study.

Soil erosion by water is sometimes considered to be a purely natural process caused by rainfall and water flow, however human activities greatly aggravate the erosion through alteration of land cover and disturbance of soil structure through cultivation. Today land use and land cover change is a significant driving agent of global change (LUCC, 1996). Such large-scale land use changes through deforestation, expansion of agricultural land and so on, as well as other human activities, are inducing changes in global systems and cycles. Land use change directly affects the atmospheric cycle and climate change, and the major external agents of water erosion vary with both changes in land use and the climate. Studies on the variation of water erosion with reference to land use and climate change will help people better understand the erosion phenomena, such that appropriate conservation countermeasures can be implemented. Projections of future soil erosion under global warming will provide us with an estimate of the most serious conceivable situations for future planning.

In the last few decades, researchers have developed models for water erosion assessment. Although their applicability varies with geographical settings, the models use common physical parameters, i.e. slope, precipitation, vegetation cover and soil erodibility, found to be important from observational experience or multivariable statistical analyses (Siakeu and Oguchi, 2000). Study of water erosion at the global scale requires investigation of the spatial variability of factors affecting the erosion processes. Recent developments of global observation by remote sensing can help to grasp the spatial distribution of vegetation. Using a digital elevation model (DEM), it is possible to extract topographical parameters from global GIS data sets. Based on the FAO–UNESCO global digital soil map (FAO, 1995), the global data set of soil properties has been made available by the Data and Information System (DIS) framework activity of the International Geosphere–Biosphere Programme (IGBP) (Scholes *et al.*, 1995). These efforts have made the global assessment of soil erosion possible at the present time.

The Revised Universal Soil Loss Equation (RUSLE) is a revision and update of the widely used Universal Soil Loss Equation (USLE) (Renard *et al.*, 1997). RUSLE uses four independent variables, rainfall erosivity, soil erodibility, topography and vegetation to estimate long-term soil loss more accurately than USLE. It is possible to expand the RUSLE model to the global scale with proper estimation of these erosion factors. A limitation of RUSLE is that sedimentation processes are neglected in the equation (Siakeu and Oguchi, 2000). RUSLE does not estimate the amount of sediment leaving a field or watershed, instead estimating soil movement at a particular site. In this study a GIS-based RUSLE is employed to simulate average annual water erosion on 0·5° grids at the global scale. The annual erosion value of a 0·5° grid refers to the average value of annual soil erosions from different hillslopes in this grid, but does not mean the amount of sediment leaving the grid. Therefore, the water erosion estimated in this study is the potential value of soil erosion. Due to a lack of global observations for model validation, present research focuses on global erosion patterns and variation trends rather than absolute erosion amounts. The main objective of this study is to offer a global view of present soil erosion potential, to analyse the trend of soil erosion over the past century, and to project the most serious possible changes of soil erosion with reference to global changes of land use and climate.

METHODOLOGY

Distributed approach to using RUSLE at the global scale

This methodology presents a 0·5° gridded estimation of annual water erosion using the RUSLE model at the global scale, supported by a number of available global data sets and the GIS commercial software ARC/INFO. Topography was simulated through the use of a DEM using the USGS HYDRO1k data set of 1-km resolution (http://edcdaac.usgs.gov/gtopo30/hydro/). Present land cover was obtained from the USGS

Global Land Cover Characteristics Data Base Version 2·0 (http://edcdaac.usgs.gov/glcc/globe_int.html) in 1-km resolution. Soil properties were obtained from the FAO global soil data set at a resolution of 5 min (FAO, 1998).

Because a linear relationship is used in the RUSLE to calculate annual soil erosion (Renard *et al.*, 1997), this study estimates the average value of potential annual erosion in 0·5° resolution by multiplying the area average erosion factors in each grid. Annual potential soil erosion of a grid located at (i, j) is estimated as

$$A(i, j) = R(i, j) \times LS(i, j) \times K(i, j) \times C(i, j) \times P(i, j) \tag{1}$$

where A is the average annual potential soil erosion (ton ha^{-1} year^{-1}) of the grid located at (i,j), R is the average rainfall erosivity factor (MJ mm ha^{-1} h^{-1} year^{-1}), LS is the average topographical parameter, K is the average soil erodibility factor (ton ha h ha^{-1} MJ^{-1} mm^{-1}), C is the average land cover and management factor, and P is the average conservation practice factor.

Slope length and steepness: LS factor. The effect of topography on soil erosion in RUSLE is accounted for by the LS factor. It contains two subcomponents: the length factor (L) and the steepness factor (S) (Renard *et al.*, 1997). The slope length factor (L) is given by

$$L = \left(\frac{\lambda}{22{\cdot}13}\right)^m \tag{2}$$

where λ is the slope length (m), m is the slope-length exponent, given as

$$m = \frac{F}{(1+F)} \quad \text{and} \quad F = \frac{\sin\beta/0{\cdot}0896}{3(\sin\beta)^{0{\cdot}8} + 0{\cdot}56} \tag{3}$$

in which β is slope angle. The slope steepness factor (S) is calculated from

$$S = \begin{cases} 10{\cdot}8\sin\beta + 0{\cdot}03, & \tan\beta < 0{\cdot}09 \\ 16{\cdot}8\sin\beta - 0{\cdot}50, & \tan\beta \geq 0{\cdot}09 \end{cases} \tag{4}$$

Slope length is defined in the RUSLE as the horizontal distance from the origin of overland flow to the point where deposition begins, or where runoff flows into a defined channel. Erosion increases as slope length increases and soil loss increases more rapidly with slope steepness than it does with slope length. The slope length and steepness derived from the DEM depend on the spatial resolution. For accurate estimations of slope length and angle, a high-resolution DEM is needed. Molnar and Pierre (1998) examined the effect of DEM resolution (from 30 m to 6 km) on the estimation of soil erosion in a catchment based on the USLE. In their paper, the slope length was assumed to be constant (=100 m) when the DEM resolution was larger than 100 m. It was found that the estimated soil erosion decreased with increasing DEM grid size due to smoothing of the slope gradient. Yang *et al.* (2001a) investigated the effect of DEM resolution (from 250 m to 1 km) on hillslope parameters and catchment hydrological responses. The topography tended to be flattened, i.e. the slope tended to be longer and gentler through resampling the DEM from fine resolution to coarse resolution. Surface runoff decreased as the slope angle decreased in a coarser resolution DEM. Figure 1 shows the sensitivity of the LS factor to the slope length and steepness. Due to opposite trends of the LS factor varying with slope length and angle, it is assumed that the effect on the LS factor that combines both slope length and angle can be compensated by the longer length and smaller angle extracted from the DEM with coarse resolutions.

In the continental hydrological model developed by Yang *et al.* (2001b), the geomorphological properties of river-hillslope formation were used to represent sub-grid topography. It is assumed that a 0·5° grid composes a set of hillslopes located along the rivers. From the macro-scale sense, the hillslopes located in a 0·5° grid are viewed as geometrically similar. The hillslope length λ is calculated as the grid area divided by the total

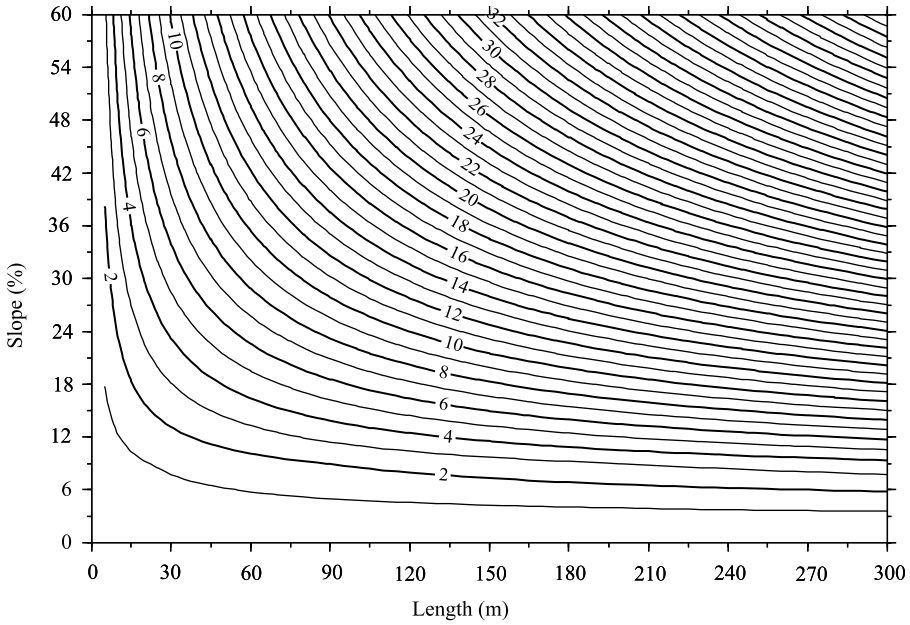

Figure 1. Sensitivity of *LS* factor

length of the streams in the same grid. Slope angle β is taken to be the mean angle of all sub-grids in the steepest direction. The same method is employed in this study.

Soil erodibility: K factor. The K factor represents average long-term soil and soil-profile response to the erosive power associated with rainfall and runoff. The RUSLE estimates the K factor using soil properties that are most closely correlated with soil erodibility (Renard *et al.*, 1997). These soil parameters are soil texture, content of organic matter, soil structure and permeability. Torri *et al.* (1997) examined a global data set of the soil erodibility factors from 596 soil samples in 86 studies. Using the field measured data, a regression equation for calculating the soil erodibility was proposed as

$$K = 0{\cdot}0293(0{\cdot}65 - D_G + 0{\cdot}24D_G^2)\exp\left\{-0{\cdot}0021\frac{OM}{f_{clay}} - 0{\cdot}00037\left(\frac{OM}{f_{clay}}\right)^2 - 4{\cdot}02CLA + 1{\cdot}72f_{clay}^2\right\} \quad (5)$$

where D_G is defined as

$$D_G = -3{\cdot}5f_{sand} - 2{\cdot}0f_{silt} - 0{\cdot}5f_{clay} \quad (6)$$

and K is in [ton ha h ha^{-1} MJ^{-1} mm^{-1}], OM is percent organic matter, f_{sand} is the fraction of sand (particle size of 0·05–2·0 mm), f_{silt} is the fraction of silt (particle size of 0·002–0·05 mm), and f_{clay} is the fraction of clay (particle size of 0·00 005–0·002 mm). Another method of estimating the soil erodibility factor used in the EPIC model (Sharpley and Williams, 1990) is employed for a simple verification. In the EPIC model, water erosion is calculated using the USLE and the soil erodibility factor [ton ha h ha^{-1} MJ^{-1} mm^{-1}] is estimated by

$$K = \frac{1}{7{\cdot}6}\{0{\cdot}2 + 0{\cdot}3\exp\left[-0{\cdot}0256SAN\left(1 - \frac{SIL}{100}\right)\right]\}\left(\frac{SIL}{CLA + SIL}\right)^{0{\cdot}3}$$
$$\left(1{\cdot}0 - \frac{0{\cdot}25OM}{OrgC + \exp(3{\cdot}72 - 2{\cdot}95OM)}\right)\left(1{\cdot}0 - \frac{0{\cdot}7SN}{SN + \exp(-5{\cdot}51 + 22{\cdot}9SN)}\right) \quad (7)$$

where $SN = 1{\cdot}0 - SAN/100$ and SAN, SIL, CLA and OM are the percentage content of sand, silt, clay and organic matter, respectively.

Information required to determine the K factor is obtained from the Digital Soil Map of the World and Derived Soil Properties, available on CD-ROM (FAO, 1998). This global soil map is developed with a 5-min resolution using the FAO/UNESCO soil classification, and the soil properties are derived corresponding to each soil type. The soil texture and organic matter content of topsoil (0–30 cm) are used to calculate the K factor at a 5-min resolution. The mean value of the K factor in a $0{\cdot}5^{\circ}$ grid is calculated by area averaging. The global K factors calculated using Equation (5) have a mean value of 0·0318 and range from 0·0 to 0·053. A very close result is given by Equation (7) as the mean value of 0·051 ranging from 0·011 to 0·051. The K factor estimated using Equation (5) is used for calculating soil erosion.

Rainfall erosivity: R factor. Rainfall erosivity, the R factor is computed originally from rainfall amount and intensity. This factor represents the driving force of sheet and rill erosion by rainfall and runoff. In order to overcome the obstacle of estimating regional R factors without sufficient long-term records of rainfall intensity, many researches have tried to establish relationships between the R factor and available precipitation data, such as monthly and annual total precipitation (Renard and Freimund, 1994; Renard *et al.*, 1997). By Renard and Freimund's work, a regression relationship between annual precipitation and the R factor has been derived based on 155 stations in the United States. This equation is written as

$$\begin{aligned} R &= 0{\cdot}0483P_a^{1{\cdot}610}, \qquad P_a \leq 850 \text{ mm} \\ R &= 587{\cdot}8 - 1{\cdot}219P_a + 0{\cdot}004105P_a^2, \qquad P_a > 850 \text{ mm} \end{aligned} \tag{8}$$

where the R factor is in [MJ mm ha^{-1} h^{-1} year^{-1}] and P_a is annual precipitation in mm. In order to obtain regional relationships between rainfall erosivity and annual precipitation, several studies performed in other regions have been reviewed (Millward and Mersey, 1999; Lal, 1990; Arnoldus, 1980; Sauerborn *et al.*, 1999). But these studies used different periods and lengths of data records over regions of various sizes, and it is difficult to verify the derived regression equations from the same base. Therefore, this research uses Equation (8) only for calculating global rainfall erosivity. This might introduce some errors for regions that have different climate characteristics from North America, but it can offer a uniform standard for evaluating global soil erosion.

Land use and conservation practice: C, P factors. For representing the effect of land use and erosion conservation practice, RUSLE uses the C factor to express the effect of cropping and management and the P

Table I. Land cover classification and C, P factors

Land cover of RUSLE	C factor	P factor
Urban area	0·1	1·0
Bare land	0·35	1·0
Dense forest	0·001	1·0
Sparse forest	0·01	1·0
Mixed forest and cropland	0·1	0·8
Cropland	0·5	0·5
Paddy field	0·1	0·5
Dense grassland	0·08	1·0
Sparse grassland	0·2	1·0
Mixed grassland and cropland	0·25	0·8
Wetland	0·05	1·0
Water body	0·01	1·0
Permanent ice and snow	0·001	1·0

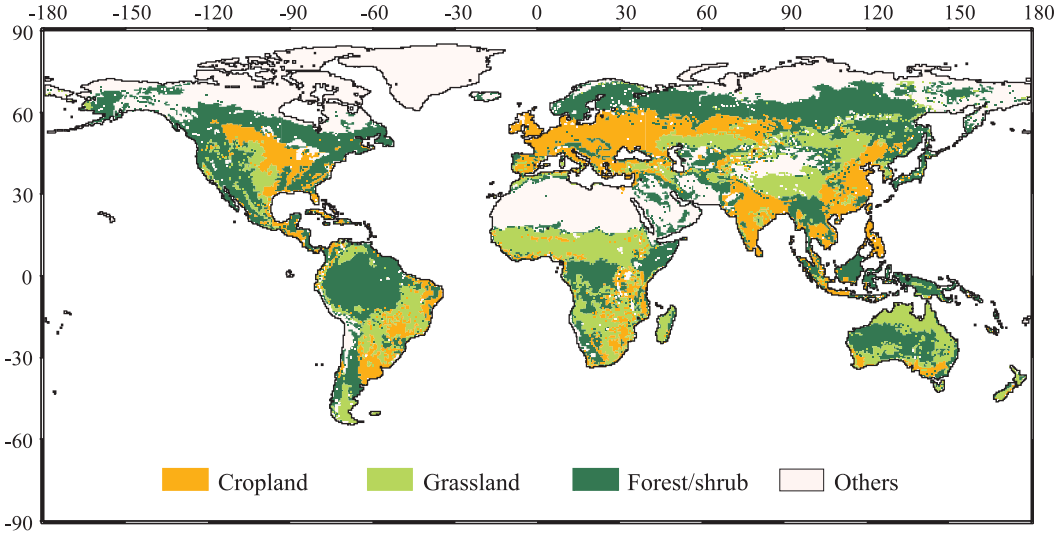

Figure 2. Present global land use

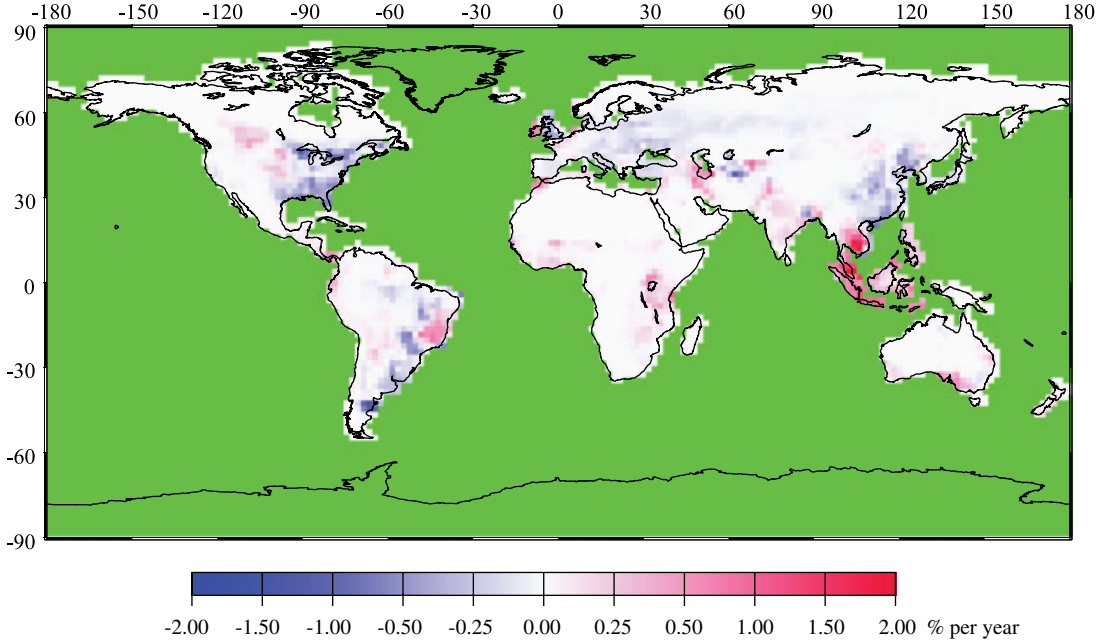

Figure 3. Changing trend of cropland in 1980s

factor for support practices (Renard *et al*., 1997). The values of *C* and *P* factors are related to the land use identified by land cover type. Land cover originally categorized by the USGS global ecosystems legend is reclassified into 13 types according to their similarity (Table I). RUSLE uses a sub-factor method to compute soil-loss ratios, which are the ratios of soil erosion at any given time in the vegetation-management sequence to soil erosion under standard conditions. The value of the *C* factor is the average soil-loss ratio weighted by the distribution of rainfall during the year. Some sub-factors used to compute the soil-loss ratio value are

difficult to obtain at the global scale. Referring to the USDA Handbook No. 282 (1981), an average value of the C factor is given to each land cover type in Table I, which corresponds to average annual canopy coverage. The monthly change of canopy represented by the leaf area index (LAI) is estimated from the NDVI data together with the vegetation type (Sellers *et al.*, 1996). The C factor value in Table I is for the annual mean LAI, and is assumed to decrease and increase linearly with LAI in different months. The annual mean value of the C factor is calculated from the monthly precipitation-weighted value.

The P factor in RUSLE is the ratio of soil erosion with a specific support practice to the corresponding soil loss with straight-row upslope and downslope tillage. The P factor accounts for control practices that reduce the erosion potential of the runoff by their influence on drainage patterns, runoff concentration, runoff velocity and hydraulic forces exerted by runoff on soil (Renard *et al.*, 1997). Human intelligence on soil erosion control is important to include in the P factor, but there is no global reference because erosion control is a very local activity. In this study, a P factor is introduced to the agricultural practice only: 0·5 for the complete agricultural land (dry crop and paddy) and 0·8 for the mixture of agricultural land with forest or grassland. Both the C and P factors are calculated based on the 1-km resolution land use data, and then averaged over each 0·5° grid.

Global changes of land use and climate

The scenarios of land use change include the historical land uses of the twentieth century, future land uses and potential land uses under present climate conditions (Ramankutty and Foley, 1998). Historical climate in the twentieth century (New *et al.*, 1999, 2000) and the future climate simulated with global warming are considered as the scenarios for climate changes.

Present global land use is obtained from the USGS Global Land Cover Characteristics Data Base in 1-km resolution (Moody and Strahler, 1994; Loveland *et al.*, 2000). As shown in Figure 2, the present global land use situation is such that forest/shrub cover is 34·9%, grassland cover is 6·8% and cultivated field cover is 14%. This data is used as the basis for deriving historical and future land uses. The historical land uses in the last century (from the 1900s to 1980s) are derived with reference to historical cropland data developed by Ramankutty and Foley (1999), which gives the gridded fraction of cropland area at 0·5° resolution from 1700 to 1992. For land development, it is assumed that the cropland was either developed from the original land covers in the order of grassland, forest, bare land, wetland, water body, snow and ice cover, or that cropland returns back to grassland. The historical land covers are estimated based on present land use and cropland data.

Some attempts have been made to model future changes in land use mainly in the developed world by building upon assumptions regarding future economic conditions and land suitability. Expert extrapolation from current practices is, however, probably the only presently feasible approach for most areas of the world (Favis-Mortlock and Guerra, 1999). Using the trends of cropland changes in a recent decade (1981–1990) shown in Figure 3, the area distributions of future croplands are calculated; then the future land uses are derived using the cropland development assumption mentioned above. The potential land cover under present climate conditions (Ramankutty and Foley, 1998) is used for isolating the natural condition from human activity.

For historical climate conditions of the twentieth century, a 0·5° gridded monthly data set developed by New *et al.* (1999, 2000) was used, which uses decade mean values of the climate parameters studied. The future change of climate is simulated using an Atmospheric GCM of high resolution based on the CGCM simulation with modest resolution under the assumption of global warming (Emori *et al.*, 1999). The simulated future climate employed in the study is approximately a 1·1° resolution. Climate changes (both precipitation and temperature) are simulated using greenhouse gas integration, which are calculated using the difference between two mean values under double CO_2 (2090–2099), according to the IPCC (1996) IS92a scenario and historic CO_2 (1980–1989) conditions. Figures 4 and 5 show the predicted changes of annual precipitation and mean temperature, respectively. The GCMs can simulate reasonable changing trends of future climate

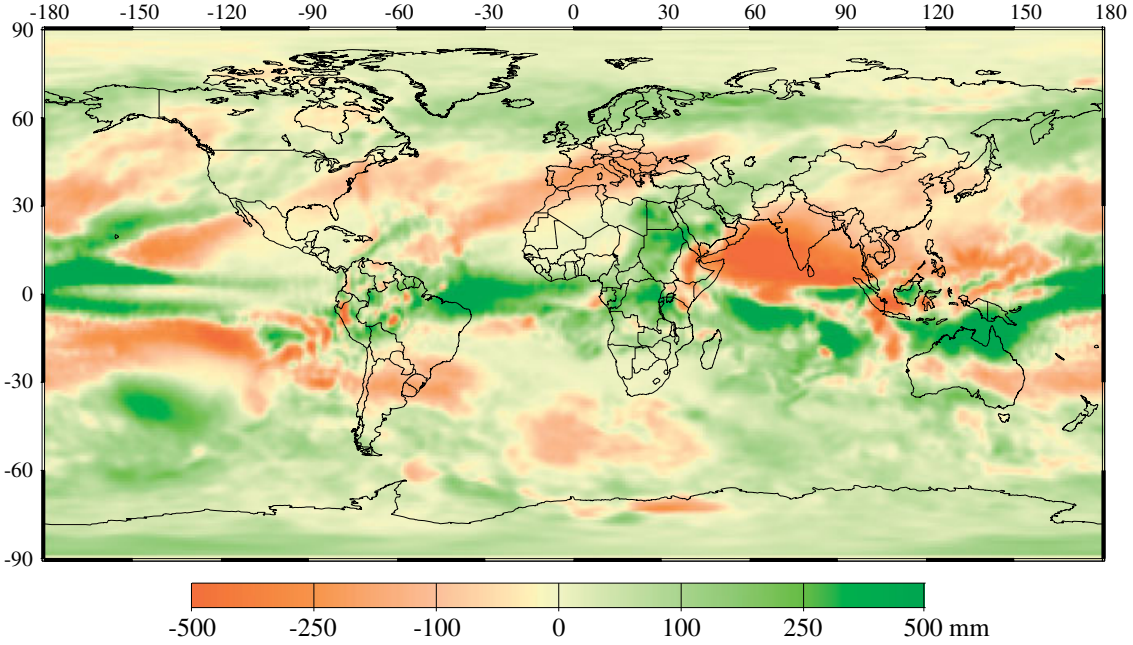

Figure 4. Simulation of precipitation change with double CO_2 concentration (annual precipitation in mm)

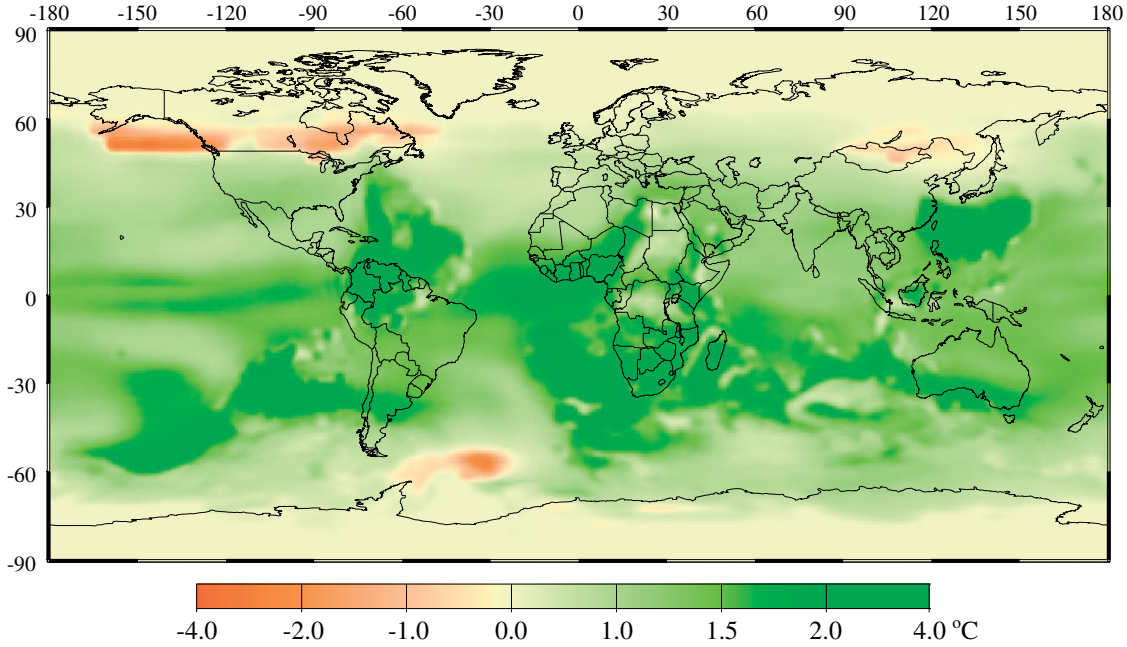

Figure 5. Simulation of temperature change with double CO_2 concentration (annual mean temperature in °C)

Table II. Scenarios used in simulation of soil erosion with reference to global changes

	Historical climate (1900s–1980s)	Present climate (1980s)	Predicted climate in 2090s (double present CO_2)
Historical land use (1900s–1980s)	Historical soil erosion (notated by H)		
Present land use (1980s)		Current soil erosion (notated by C)	Future soil erosion due to climate change (notated by D)
Potential vegetation under present climate		Soil erosion under potential vegetation (notated by P)	
Future land use (2090s)		Future soil erosion with land use change (notated by F)	Future soil erosion due to both land use and climate changes (notated by E)

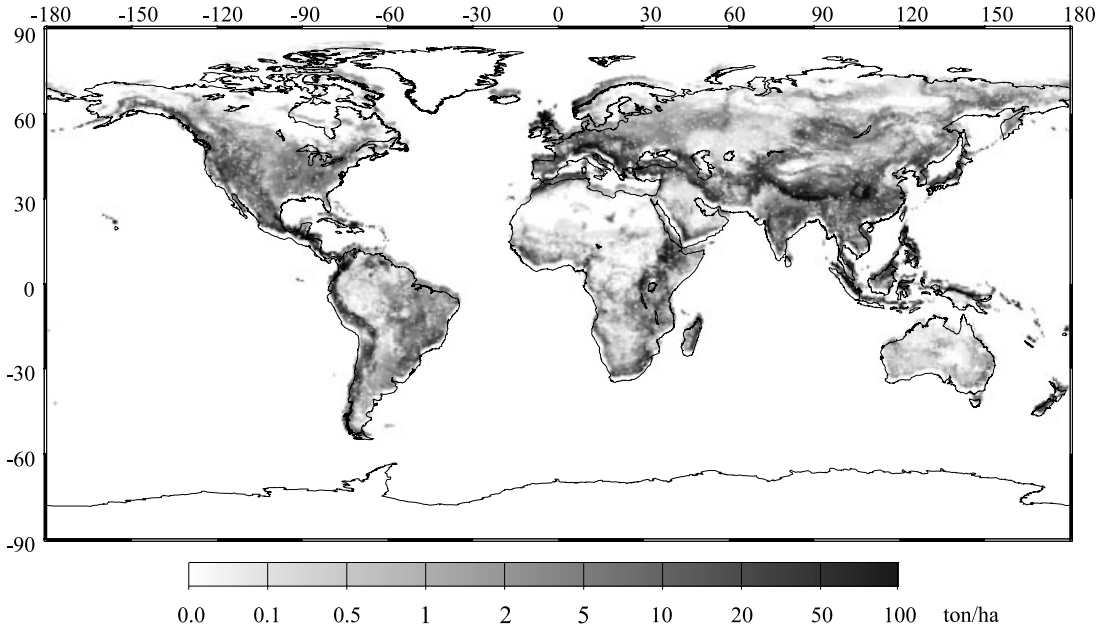

Figure 6. Present global annual soil erosion potential

but are highly uncertain regarding the absolute value of precipitation, and therefore the climate in the 2090s is estimated by adding the GCM simulated changes after global warming to the present climate condition.

The results of simulations of potential soil erosion by water, made through considering the changes of land use and climate, are shown in Table II. They are (1) C—current soil erosion based on current land use and climate; (2) H—historical soil erosion based on historical land use and climate; (3) P—soil erosion based on potential vegetation cover under present climate; (4) F—future soil erosion with changing land use; (5) D—future soil erosion with changing climate; and (6) E—future soil erosion due to both changes of land use and climate.

Table III. Present mean value of potential soil erosion in each region (unit: ton ha^{-1} $year^{-1}$)

Region	1900s	1910s	1920s	1930s	1940s	1950s	1960s	1970s	1980s	2090s
Whole world	8·7	8·9	8·9	9·3	9·3	9·7	9·9	10·1	10·2	11·6
Continents										
Africa	3·8	3·7	3·8	3·9	3·8	4·2	4·5	4·5	4·4	6·0
Asia	10·4	10·8	10·8	11·2	11·3	11·8	12·0	12·0	12·2	14·4
Australia	2·4	2·4	2·5	2·4	2·7	2·7	2·8	3·1	3·0	4·1
Europe	10·7	11·4	11·2	11·6	10·7	11·5	11·6	11·6	11·1	8·9
North America	6·8	6·8	6·9	7·5	7·9	8·3	8·8	8·9	9·3	10·0
South America	6·1	6·3	6·4	6·8	7·0	7·0	7·2	8·2	8·5	10·3
Selected countries										
United States	7·5	7·5	7·3	7·3	7·7	7·0	7·2	7·1	6·9	7·6
Brazil	2·1	2·1	2·3	2·3	2·5	2·5	3·0	3·8	4·3	4·9
China	14·9	15·6	14·9	15·1	15·0	15·0	15·0	14·9	14·7	14·2
India	14·3	15·1	15·3	16·2	16·6	17·1	16·6	16·8	16·8	15·5
Thailand	5·5	5·8	6·5	7·8	9·0	10·4	12·2	13·4	14·1	17·3
Selected basins										
Mississippi	4·7	5·0	4·9	4·2	4·9	4·3	4·3	4·2	4·1	4·3
Amazon	3·4	3·6	3·6	3·8	3·9	3·8	4·1	4·8	5·0	6·2
Nile	4·1	4·0	4·1	4·3	4·4	4·7	5·2	5·0	4·9	8·8
Amur	2·3	2·3	2·3	2·6	2·4	2·8	2·6	2·5	2·6	2·5
Huanghe	7·7	7·8	7·2	7·8	7·6	7·7	8·2	7·4	7·5	6·2
Yangtze	29·1	31·0	28·8	29·5	29·3	30·0	29·9	29·5	29·1	26·5
Mekong	7·3	7·1	7·7	7·8	8·9	8·6	9·5	9·0	9·6	13·0
Ganges	38·3	40·7	40·0	40·8	40·9	39·7	40·1	41·0	42·2	40·7
Indus	20·6	19·8	20·9	19·5	19·6	22·3	21·1	21·0	21·5	20·4

RESULTS AND DISCUSSION

All simulations designed in Table II were carried out using the above method. Using a limited number of statistical data, Pham *et al.* (2001) carried out a simple verification in the pre-study of present global water erosion. Present estimation of global soil erosion was initially compared with the global sediment yields from major rivers of the world (Walling and Weep, 1987). A map of global sediment yield has been introduced by Walling and Weep (1987). In this map, only the suspended sediment yields in some main rivers of the world have been included. The amounts of sediments counted in this map are the sediments moving from small fields into local rivers as suspended loads. This data cannot be used directly for validation of present simulation of global erosion. However, it provides a means of checking the reasonableness of the present global estimation. The pattern of sediment yields in this map agrees with the distribution of soil erosion in the present study. Both indicate that Southeast Asia has the most serious soil erosion problems. Present estimation of soil erosion shows more variability than that in Walling and Weep's sediment yield map.

Present status of global potential soil erosion

The global pattern of present soil erosion obtained from simulation C is shown in Figure 6. There are two strong soil erosion zones: one lies along the west coast line from North America to South America; another is from South Europe to the Middle East and Southeast Asia. The most serious erosion is in Southeast Asia. The spatial distribution of high soil erosion is closely related to mountainous areas located in the tectonic zones and dense croplands of the high population regions. This implies that both natural geomorphology and human activity are major factors for inducing soil erosion. The global average value of present potential erosion is estimated to be 10·2 ton ha^{-1} $year^{-1}$. This means approximately 0·38 mm $year^{-1}$ (assuming 2·65 ton m^{-3} bulk density) depth of topsoil on the earth is moving from its original location, with a portion transported to

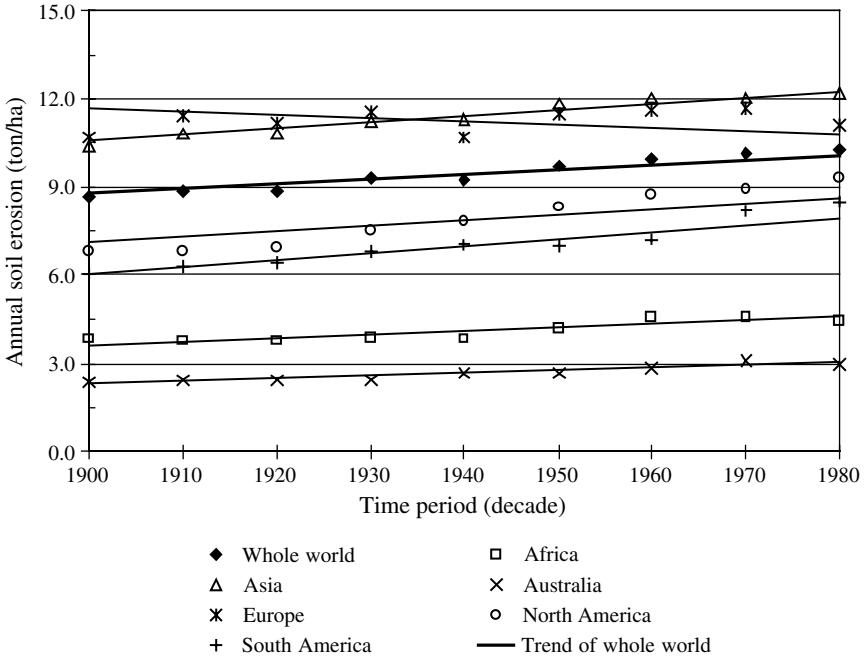

Figure 7. Historical trend of soil erosion potential over the last century

Table IV. Comparing the changes of soil erosion in the twentieth century

	Whole world	Africa	Asia	Australia	Europe	North America	South America
Change of population (%)[a]	141·3	266·1	163·1	140·0	33·3	79·8	182·5
Change of cropland (%)[b]	51·1	66·2	45·8	398·0	26·7	37·7	414·0
Change of annual soil erosion, ton ha^{-1} (%)[c]	1·5 (17)	0·6 (16)	1·8 (17)	0·6 (25)	0·4 (4)	2·5 (37)	2·5 (41)

[a] This is the change of population from 1950 to 2000.
[b] This is the change of cropland from the 1900s to the 1980s.
[c] This is the change of soil erosion by water from the 1900s to the 1980s.

rivers, lakes and oceans. High soil erosion must cause high deposition of sediment in rivers and lakes, and this is one of the major reasons for floods and water pollutions. The great flood in the Yangtze River basin of China in 1998 is an example (Yin and Li, 2001).

Historical trend of soil erosion over the last century

Simulations of historical changes of potential soil erosion have been carried out from 1901 to 1990 (simulation H). Decadal average results are summarized in Table III and are also shown in Figure 7. It can be seen that soil erosion at the global scale was increased during the last century. A common increasing trend has been found in all continents except Europe. The simulated annual soil erosion over the last century increased about 1·5 ton ha^{-1} at the globe, 0·6 ton ha^{-1} in Africa, 1·8 ton ha^{-1} in Asia, 0·6 ton ha^{-1} in the Australia–Pacific region, 0·4 ton ha^{-1} in Europe, 2·5 ton ha^{-1} in North America and 2·4 ton ha^{-1} in South America. The regions with the largest increases are in the tropic rain

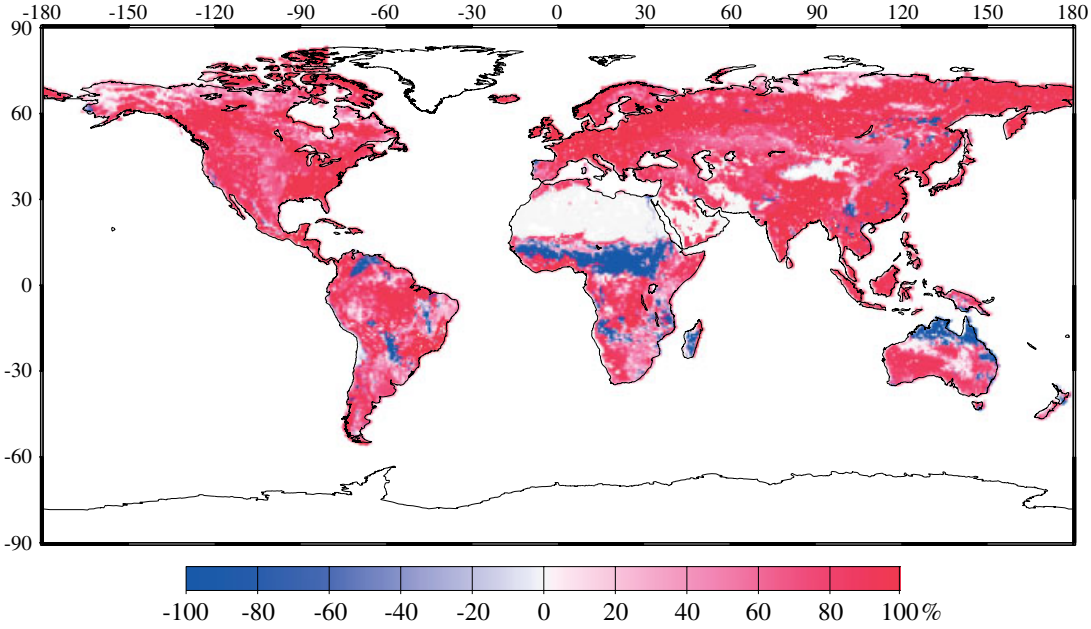

Figure 8. Human effect on potential soil erosion: (simulation C−simulation P)/simulation C

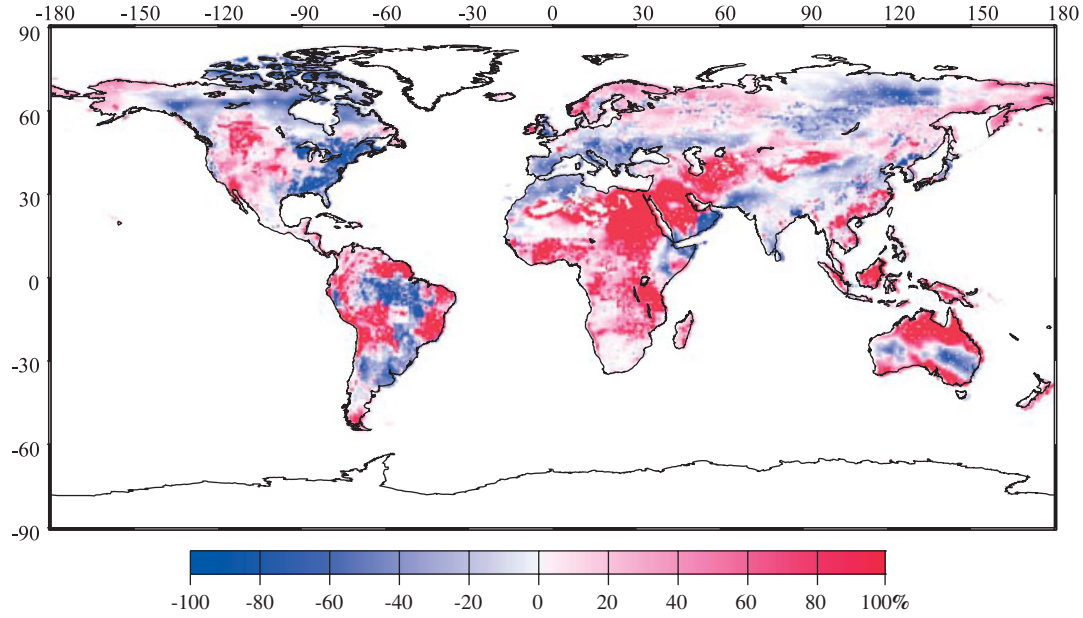

Figure 9. Projection of soil erosion change in the 2090s: (simulation E−simulation P)/simulation C

forest regions, such as Brazil, Thailand and the lower Mekong basin. By comparing with the population and cropland (see Table IV), the trend of simulated soil erosion agrees with the trends of population and cropland except for North America (WRI, 1998a,b). This agreement between soil erosion trend and population and cropland trends indicates that human activity is the major factor causing the

Table V. Mean change of soil erosion in each region under different conditions

	Change by human activity (%) (C − P)/C	Change in twenty-first century (%)		
		Total change (E − C)/C	By land use (F − C)/C	By climate (D − C)/C
Whole world	60·3	13·9	5·3	9·0
Continents				
Africa	23·9	36·2	18·8	15·7
Asia	71·0	11·9	3·6	8·2
Australia	43·0	51·1	8·0	42·4
Europe	87·9	−4·9	−7·7	3·9
North America	75·2	−6·9	−4·5	−2·2
South America	60·0	12·2	7·8	6·3
Selected countries				
United States	76·4	−1·5	−11·5	9·3
Brazil	63·8	−2·7	−7·2	9·4
China	71·8	5·8	3·9	1·5
India	85·2	−14·4	−2·6	−12·4
Thailand	84·9	24·8	39·5	−11·9
Selected basins				
Mississippi	77·9	5·6	−1·3	6·0
Amazon	71·6	6·8	2·1	8·2
Nile	−7·8	84·9	22·5	45·5
Amur	66·2	1·0	−5·2	7·6
Huanghe	73·4	−18·2	−2·7	−15·9
Yangtze	76·0	0·5	6·3	−7·8
Mekong	80·6	38·5	48·4	−9·6
Ganges	93·4	−6·2	1·8	−7·8
Indus	63·5	−14·4	−2·6	−12·4

increase of soil erosion. The exception of North America is mainly caused by shrinking agricultural lands.

Human effect on soil erosion

For evaluating the human effect on soil erosion, simulation P is carried out using the potential vegetation cover under present climate conditions. The difference between the soil erosions under current actual land cover with human activity (simulations C) and under the potential land cover without human activity (simulation P) gives a reference to the effect of human activity (Figure 8). Human activity increases soil erosion in most parts of the world. In global mean, soil erosion is increased by approximately 60% due to human activity. Human contribution to soil erosion in different continents, countries and basins is shown in Table V. It varies in a very wide range, from −8 to 90% and roughly matches the pattern of population density distribution (Tobler *et al*., 1995). Human-induced erosion reduction (blue colour in Figure 8) has been seen in simulation P, for example in the Nile basin. This is because artificial irrigation helps vegetation growth and reduces soil erosion. Regions with sparse populations are still strongly affected by human activity, such as in the Siberia and Amazon basins. Deforestation in these regions could be the main reason.

Projection of future soil erosion

Possible changes of potential soil erosion in the 2090s due to the changes of land use and climate are examined using simulations C and E. The difference between the results of simulations E and C gives the changes in soil erosion in the 2090s compared to the 1980s, as shown in Figure 9. Analyses on global,

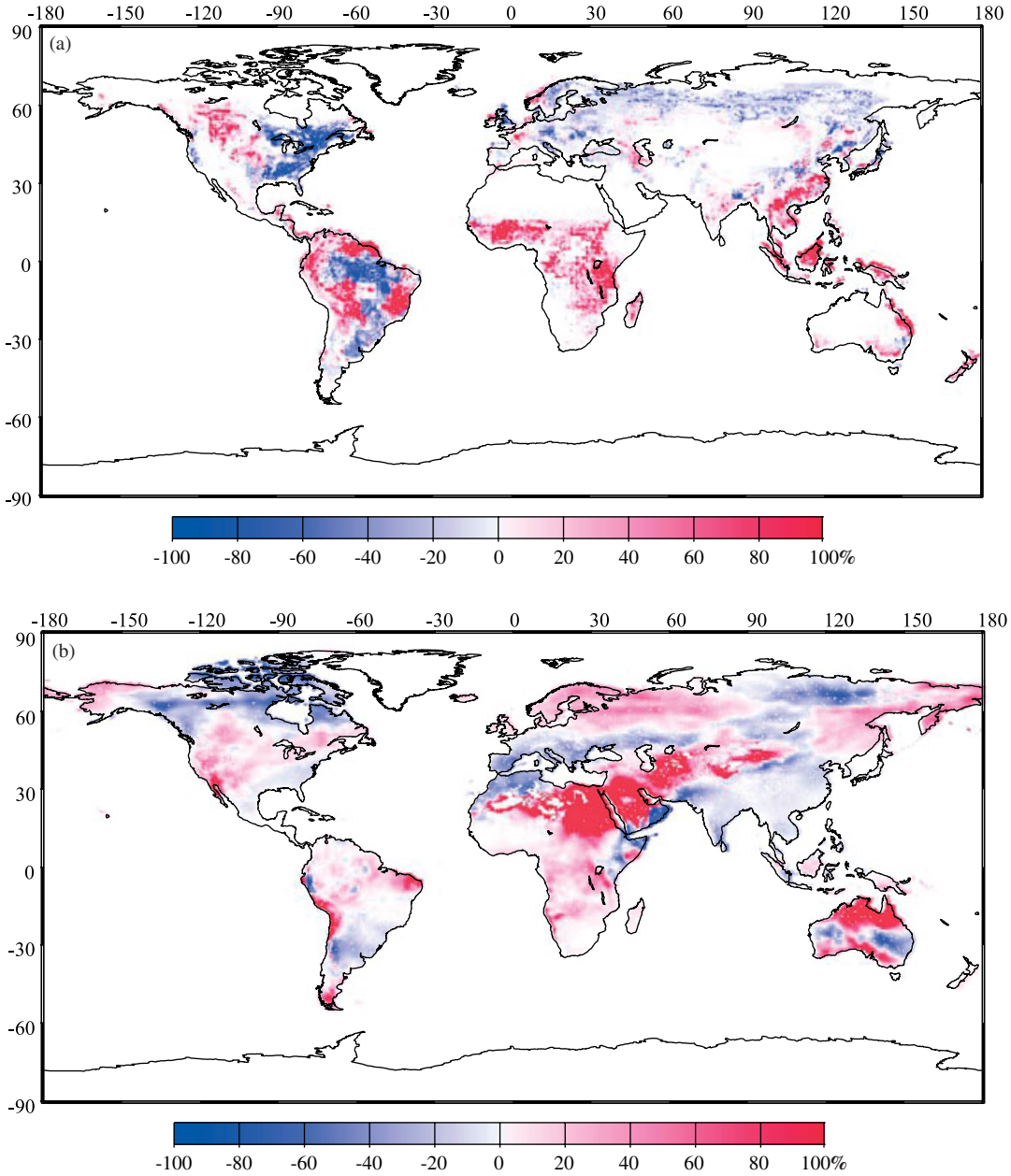

Figure 10. (a) Projection of soil erosion change in the 2090s due to land use change: (simulation F−simulation P)/simulation C. (b) Projection of soil erosion change in the 2090s due to global warming: (simulation D−simulation P)/simulation C

continental, country and basin scales are summarized in Table V. Soil erosion after 100 years in most parts of the world is projected to increase about 14% on average across the globe. At the continental scale, only Europe and North America will have a slight decrease. Australia and Africa have high increases, approximately 40−50% increase compared to the 1980s.

In order to investigate the effect of land use change and climate change, simulations F and D have been carried out respectively (Table II). The difference between the two results of simulations F and C gives the

effect of land use change (Figure 10a), and the effect of climate is estimated from the difference between D and C (Figure 10b). Generally, the effect of climate change is larger than that of land use change. Increases in soil erosion due to climate change are mainly induced by precipitation increase. In terms of the global mean, changes in soil erosion in the 2090s are projected to increase by about 9% due to climate and about 5% due to land use. Contributions to the increase in global soil erosion by climate change are nearly twice that of land use change. Projections show that soil erosion increases in the most dense population areas due to land use changes, but climate change induces a different pattern of erosion change. The regions with the same increasing trend of both population and precipitation might face more serious problems of soil erosion in the future, such as South America and Africa found in the present study.

CONCLUSION

This study successfully employed a GIS-based RUSLE model to simulate global soil erosion. It offered us the first overview of present global potential soil erosion, examined historical changes of potential soil erosion in the last century, and projected future conditions for 2090 under global changes in climate and land uses. Present soil erosion potential is estimated to be about 0·38 mm year^{-1}, and Southeast Asia is the region with the most serious erosion problem. This large amount of soil erosion is caused by, and is causing, many floods and other environmental problems. Soil erosion is a natural earth surface process, but it is accelerated by human activity, especially by land development. It was estimated that nearly 60% of present soil erosion was induced by human activity. With the development of cropland in the last century, potential soil erosion was estimated to increase by about 17%. Global warming might cause more significant increases in soil erosion than land use development in the future from the global view. The regions with the same increasing trend of precipitation and population would face increasingly serious soil erosion problems. This research is a useful step in studying global change and associated environmental problems, although there are some uncertainties in the global estimation of several erosion factors.

ACKNOWLEDGEMENTS

This research is partially supported by "Research and Development of Hydrological System Modelling and Water Resources System" on the Core Research for Evolutional Science and Technology (CREST) of the Japan Science and Technology Corporation (JST).

REFERENCES

Arnoldus HMJ. 1980. An approximation of the rainfall factor in the USLE. In *Assessment of Erosion*, DeBoodt M, Gabriels D (eds). John Wiley: Chichester, 127–132.

Bridges EM, Oldeman LR. 1999. Global assessment of human-induced soil degradation. *Arid Soil Research and Rehabilitation* **13**: 319–325.

Emori S, Nozawa T, Abe-Ouchi A, Numaguti A, Kimoto M, Nakajima T. 1999. Coupled ocean–atmosphere model experiments of future climate change with an explicit representation of sulfate aerosol scattering. *Journal of the Meteorological Society of Japan* **77**: 1299–1307.

FAO. 1995. The Digital Soil Map of the World, Version 3.5. United Nations Food and Agriculture Organization, CD-ROM.

FAO. 1998. Land and Water Digital Media Series N-1, December, ISBN 92-5-104050-8.

Favis-Mortlock DT, Guerra AJ. 1999. The implications of general circulation model estimates of rainfall for future erosion: a case study from Brazil. *Catena* **37**: 329–354.

IPCC. 1996. *Climate Change 1995: The Science of Climate Change*, Houghton JH, Meira Filho LG, Callander BA, Harris N, Kattenberg A, Maskell K (eds). Cambridge University Press: Cambridge; 572 pp.

Lal R. 1990. *Soil Erosion in the Tropics: Principle and Management*. McGraw-Hill: New York.

Lal R, Bruce JP. 1999. The potential of world cropland soils to sequester C and mitigate the greenhouse effect. *Environmental Science & Policy* **2**: 177–185.

Loveland TR, Reed BC, Brown JF, Ohlen DO, Zhu J, Yang L, Merchant JW. 2000. Development of a Global Land Cover Characteristics Database and IGBP DISCover from 1-km AVHRR Data. *International Journal of Remote Sensing* **21**(6/7): 1303–1330.

LUCC. 1996. Land Use and Cover Change (LUCC) Open Science Meeting Proceedings LUCC Report Series No. 1, Amsterdam, the Netherlands.

Millward AA, Mersey JE. 1999. Adapting the RUSLE to model soil erosion potential in a mountainous tropic watershed. *Catena* **38**: 109–129.
Molnar DK, Pierre YJ. 1998. Estimation of upland erosion using GIS. *Computers & Geosciences* **24**(2): 183–192.
Moody A, Strahler AH. 1994. Characteristics of composited AVHRR data and problems in their classification. *International Journal of Remote Sensing* **15**(17): 3473–3491.
New M, Hulme M, Jones P. 1999. Representing twentieth-century space–time climate variability. Part I: Development of a 1961–90 mean monthly terrestrial climatology. *Journal of Climate* **12**: 829–856.
New MG, Hulme M, Jones PD. 2000. Representing twentieth-century space–time climate variability. Part II: Development of 1901–1996 monthly grids of terrestrial surface climate. *Journal of Climate* **13**: 2217–2238.
Pham TN, Yang D, Kanae S, Oki T, Musiake K. 2001. Application of RUSLE model on global soil erosion estimate. *Annual Journal of Hydraulic Engineering, JSCE* **45**: 811–816.
Pimentel D, Harvey C, Resosudarmo P, Sinclair K, Kurz D, MnCair M, Crist S, Shpritz L, Fitton L, Saffouri R, Blair R. 1995. Environmental and economic costs of soil erosion and conservation benefits. *Science* **267**: 1117–1123.
Ramankutty N, Foley JA. 1998. Characterizing patterns of global land use: an analysis of global croplands data. *Global Biogeochemical Cycles* **12**(4): 667–685.
Ramankutty N, Foley JA. 1999. Estimating historical changes in global land cover: croplands from 1700 to 1992. *Global Biogeochemical Cycles* **13**(4): 997–1027.
Renard KG, Freimund JR. 1994. Using monthly precipitation data to estimate the R-factor in the revised USLE. *Journal of Hydrology* **157**: 287–306.
Renard KG, Foster GR, Weesies GA, McCool DK, Yoder DC. 1997. *Predicting Soil Erosion by Water: A Guide to Conservation Planning with the Revised Universal Soil Loss Equation (RUSLE)*. Handbook **703**, US Department of Agriculture, 404 pp.
Sauerborn P, Klein A, Botschek J, Skowronek A. 1999. Future rainfall erosivity derived from large-scale climate models—method and scenarios for a humid region. *Geoderma* **93**: 269–276.
Scholes RJ, Skole D, Ingram JS. 1995. A global database of soil properties: proposal for implementation. *IGBP-DIS working paper No. 10*, University of Paris, France.
Sellers PJ, Randall DA, Collantz GJ, Berry JA, Field CB, Dazlich DA, Zhang C, Collelo GD, Bounoua L. 1996b. A revised land surface parameterization (SiB2) for atmospheric GCMs. Part II: The generation of global fields of terrestrial biophysical parameters from satellite data. *Journal of Climate* **9**: 706–737.
Sharpley AN, Williams JR. 1990. EPIC-Erosion/Productivity Impact Calculator: 1. Model Documentation. *USDA Technical Bulletin* **1768**: 235.
Siakeu J, Oguchi T. 2000. Soil erosion analysis and modeling: A review. *Transactions, Japan Geomorphological Union* **21**: 413–429.
Singer MJ, Warkentin BP. 1996. Soils in an environmental context: an American perspective. *Catena* **27**: 179–189.
Tobler W, Deichmann U, Gottsegen J, Maloy K. 1995. The Global Demography Project. National Center for Geographic Information and Analysis Department of Geography, University of California, Santa Barbara CA 93106-4060. *Technical Report*, TR-95-6.
Torri D, Poesen J, Borselli L. 1997. Predictability and uncertainty of the soil erodibility factor using a global dataset. *Catena* **31**: 1–22.
Walling DE, Weep BW. 1987. Material transport by the world's rivers: evolving perspectives. *IAHS Publication* **164**: 313–329.
WRI. 1998a. *World Resources 1998–99: Environmental Change and Human Health*. World Resources Institute: Oxford University Press, 384 pp.
WRI. 1998b. *World Resources 1998–99: World Resources CD-rom*. World Resources Institute: Washington, DC.
Yang D, Herath S, Musiake K. 2001a. Spatial resolution sensitivity of catchment geomorphologic properties and the effect on hydrological simulation. *Hydrological Processes* **15**: 2085–2099.
Yang D, Kanae S, Oki T, Musiake K. 2001b. Expanding the distributed hydrological modelling to continental scale. *IAHS Publication*. **270**: 125–134.
Yin H, Li C. 2001. Human impact on floods and flood disasters on the Yangtze River. *Geomorphology* **41**: 105–109.

